PROCEDURE FOR TESTING KINETIC MODELS OF THE PHOTOCYCLE OF BACTERIORHODOPSIN

JOHN F. NAGLE
Departments of Physics and Biological Sciences, Carnegie-Mellon University, Pittsburgh, Pennsylvania 15213

LUIS A. PARODI AND RICHARD H. LOZIER
Cardiovascular Research Institute and Department of Biochemistry and Biophysics, University of California, San Francisco, California 94143

ABSTRACT Given some simple kinetic models of the photocycle of bacteriorhodopsin (bR) and data taken at many wavelengths and under conditions that avoid photoselection and steady-state cycling complications, it is shown how to extract the apparent rate constants and the spectra of the intermediates. Special consideration was given to establishing the range of error of these results. There are many criteria, which we explicitly discuss, that the spectra should satisfy in order that the kinetic model be acceptable. New data for the photocycle of purple membrane fragments in dilute buffer at pH 7.0 has been obtained at 15 measuring wavelengths and four temperatures. The procedure, which can be generalized to more complex models, has been applied to these data to test two kinds of kinetic models: the unidirectional unbranched model and the unidirectional model with simple branching straight back to bR from any intermediate. In these models the spectrum of the O intermediate is highly temperature sensitive, even with branching, and/or has two broad maxima. Moreover, the spectrum of the M intermediate has a secondary maximum and two M-like states appear to be required. Thus, neither model satisfies the physical criteria.

INTRODUCTION

Establishing the kinetic model of the photocycle of bacteriorhodopsin (bR) is one of the more important steps towards an understanding of the mechanism of this light-driven proton pump (Stoeckenius et al., 1979). Knowledge of the spectra of the intermediates and their interconnection in the photocycle puts important restrictions on molecular models, especially as regards the action of the retinal, whose environment and state of protonation can be correlated with the spectra (Honig et al., 1976; Blatz and Mohler, 1975). Also, the central role of the chromophore suggests that other aspects of the molecular mechanism (e.g., protein conformational changes and protonation changes) may be kinetically linked to the photocycle seen by optical absorption spectroscopy of the chromophore. Thus, a model that fits the observed optical absorption changes should be useful in gathering and interpreting data using other techniques.

Considerable effort has been expended in measuring and attempting to understand the light-induced optical absorption changes of bR. There is substantial agreement that the cycle consists of at least four intermediates (designated K,L,M, and O). However, there has been considerable uncertainty and controversy about the kinetic model. Fig. 1 shows a sketch that includes many of the suggestions in the literature, although no one has yet suggested that the true model is so complicated that all the features in Fig. 1 are necessary. An early model proposed for the cycle consisted of intermediates K_{590}, L_{550}, M_{412}, and O_{640} (the subscript representing the position of the absorption maximum in nanometers), whose absorption spectra were calculated on the assumption of an unbranched unidirectional model (Lozier et al., 1975). Since then, additional states have been proposed. A state preceding K, designated S, has been identified by picosecond spectroscopy (Applebury et al., 1978). From kinetic resonance Raman studies a state X was proposed to occur between L and M (Marcus and Lewis, 1978). Gillbro et al. (1977) found a state P which Gillbro (1978) suggested came between O and bR in an unbranched unidirectional cycle. However, the complexity of the cycle has led others to challenge the unidirectional unbranched model. Dencher and Wilms (1975) suggested a branch from M straight back to bR bypassing O, and this model has been strongly favored by Sherman et al. (1976 and 1979). Lozier and Niederberger (1977) stated that "at least one additional path (back reaction or branch) is needed." Korenstein et al. (1978) have proposed an even more radical departure from previous models, suggesting a model that involves two L and two M states. Another radical model with two M states and an X state is favored by Edgerton and Greenwood (1979). This disagreement is

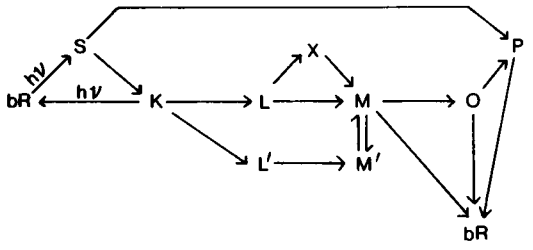

FIGURE 1 Scheme showing some of the intermediates and pathways that have been proposed for the photocycle of light-adapted bacteriorhodopsin.

far from trivial and precludes clear cut interpretations of kinetic measurements.

Preceding analyses have involved one or more assumptions that have flawed them from the outset. The first is that absorption changes at specific wavelengths are due entirely to concentration changes of specific intermediates, e.g., changes at 410 nm are due entirely to M and changes at 660 nm are due entirely to O (Sherman et al. 1976 and 1979; Korenstein et al. 1978; Gillbro, 1978). However, it is clear (Gillbro, 1978; Stoeckenius et al., 1979) that the absorbance changes at any wavelength depend upon all intermediates to varying degree, and that small changes in an intermediate whose concentration changes drastically can be interpreted as large changes in an intermediate whose concentration changes are much smaller. The second assumption is that at specific times after the flash only one intermediate is present, e.g., at 1 ms only M and unexcited bR are present (Lozier et al., 1975; Kung et al., 1975; Dencher and Wilms, 1975). Again, this assumption can lead to substantial errors in the spectra because of the presence of small concentrations of intermediates whose absorption changes are large in a particular wavelength region. In addition to these systematic assumptions, sometimes plausible-sounding criteria have been presented as obvious facts and used to draw conclusions about the model. An illustration is the statement that "the rate constants for decay of M are significantly lower than for the appearance of O. For an exclusively unbranched sequence clearly these two rate constants must be identical" (Sherman et al., 1976). As pointed out by Gillbro (1978), however, if $k_{M\to O}$ is smaller than $k_{O\to bR}$, then O appears to rise with the rate constant $k_{O\to bR}$, and one would not expect the appearance of O, as determined from a plot of the absorbance at 660 nm vs. time, to have the same rise kinetics as $k_{M\to O}$. In a later paper Sherman et al. (1979) make the valid quantitative criticism of the unbranched model that the maximum amount of O formed increases as temperature is increased. From this they again suggested that the model involves a simple M→bR branch. This latter suggestion, however, can not be tested with data at only two measuring wavelengths.

In the present paper we develop a systematic procedure that avoids the assumptions that have flawed previous analyses. We also take data at 15 measuring wavelengths, which permits testing of more complicated models. Comprehensive treatment of such extensive data requires an innovation in nonlinear least-squares analysis that was not available to previous workers.

BASIS OF THE PROCEDURE

The following outline serves to introduce the reader to the general problem of finding the kinetic model for the photocycle of bR, and the kinds of assumptions and criteria, labeled as propositions, that may be used to restrict the possible models. It is important to emphasize that the procedure we suggest in this outline relies strongly on physical criteria that must be applied judiciously; it is not just a game in statistical analysis.

The kinetic development of the absorbance change of the sample after a fast flash contains information about the rate constants and the spectra of the intermediates. In particular, assuming first-order or pseudo-first-order kinetics and no degenerate rate constants, one has the following at time t.

Proposition I:

$$A(t,\lambda) = \sum_{i=1}^{NL} b_i(\lambda) e^{-k_i t}. \qquad (1)$$

Here $A(t,\lambda)$ is the relative absorbance, i.e., with the absorbance $A_{bR}(\lambda)$ of bR subtracted from the measured absorbance $A_m(t,\lambda)$. The k_i are the apparent rate constants, of which there are NL if there are NL intermediates. The linear amplitudes, b_i, depend upon measuring wavelength and are related in a model-dependent way to the difference spectra of the intermediates $\epsilon_i'(\lambda) = \epsilon_i(\lambda) - \epsilon_{bR}(\lambda)$, $i=1,...NL$. The spectra of the intermediates K, L, and M have been studied at very low temperatures, so that their gross features are known, although there is not complete quantitative agreement between different groups (Becher et al., 1978; Iwasa et al., 1981). Furthermore, quantitative aspects of the spectra may change slowly with temperature. For example, the liquid nitrogen spectrum of K does not agree with the one we find at room temperature (see below). Therefore, we do not use the low-temperature spectra in our analysis, although it is useful to compare them with our results at the end, and it is encouraging that the low-temperature spectra of L and M, which are observed at temperatures closer to room temperature than the K spectrum, do agree reasonably well with our spectra.

The first problem in the analysis of the data is that there may be other physical kinetic effects, such as tumbling of the membrane fragments in suspension or orientation shifts of the chromophore in the intermediates, which, because of photoselection, lead to different relations between b_i and the spectra than would be predicted by any chemical kinetic model of the sort sketched in Fig. 1.

These particular problems have been avoided by the use of magic angle polarizers, as discussed in Methods. Although this guarantees that the relation between b_i and the spectra depend only upon the chemical kinetic model, if the measuring beam is strong enough to be actinic so that there is a significant fraction cycling in the steady-state, the relations between the b_i and the spectra change, becoming more complex, as discussed in Methods. We have avoided this complication by using low light levels in the measuring beam.

If one assumes that Eq. 1 represents the data, the first problem in the analysis is one of nonlinear least-squares fitting to determine b_i and k_i. Details are discussed below in Analytical Methods, but it is worth mentioning here one feature of our procedure that we feel is especially advantageous. Instead of doing nonlinear least-squares on the kinetic traces of each measuring wavelength separately, we do all wavelengths simultaneously, and force the solution to have the same rate constants k_i for all λ. The restriction that the k_i be the same for all λ is a fundamental one with which the data must agree. Furthermore, by employing this fundamental restriction, the results of the statistical analysis are much easier to interpret.

The first question that is addressed by the statistical analysis is how many intermediates (*NL* in Eq. 1) are there? This question can be addressed by examining the residual errors between the data and the best fit of Eq. 1, given *NL*, not only as a function of time but also as a function of wavelength λ. The residual errors may look nonrandom as a function of time at one λ. If, however, the nonrandomness is not similar at other close measuring wavelengths, namely if the errors do not occur at the same time with the same sign and smoothly varying amplitudes as a function of λ, then more intermediates, *NL*, are not called for. This analysis is based on an important physical assumption:

Proposition II: The spectra of each intermediate should be smoothly varying over the wavelength grid employed.

The wavelength grid used has 20-nm intervals from 380 to 680 nm, excluding 500 nm and sometimes 480 and 520 nm owing to very large flash artifacts at these wavelengths. The spectra of most retinal compounds, including the low temperature spectra of bR, are fairly smooth on this grid. Following this analysis, one may very easily see that $NL=3$ is not enough intermediates and that $NL=4$ is plausible. There are, however, other criteria that may raise *NL* beyond 4, as will be discussed later.

Even when the minimal *NL* and the corresponding values of k_i and b_i are found, there are very many kinetic models that can be made to fit, as discussed below in Kinetic Model Analysis. There are surprisingly many, however, that can be eliminated by the following two criteria:

Proposition III: All spectra of the intermediates must have only positive extinctions $\epsilon_i(\lambda)$.

That is, the intermediates are not significantly fluorescent in the 380–680-nm range. But owing to low signal-to-noise at the extreme wavelengths, the computed $\epsilon_i(\lambda)$ may be allowed to become slightly negative at an occasional wavelength in regions where $\epsilon_i(\lambda)$ is small.

Proposition IV: The fraction cycling *FC* for a kinetic model must agree with the measured value and must certainly not exceed unity.

The measured value of the fraction cycling is somewhat uncertain as discussed in Results. However, most of the possible models require the fraction cycling to exceed unity and can be dismissed absolutely. Only a few eliminations require more accurate values of *FC*.

Temperature is a very important variable in our analysis. There are three temperature-related assumptions for kinetic models. Of course, the kinetic constants are strongly temperature dependent and it is customary to assume the following:

Proposition V: The k_i in kinetic models should have linear Arrhenius plots. There is, however, a strong reservation about this proposition. Although there is no detectable bulk phase transition as shown by differential scanning calorimetry (Jackson and Sturtevant, 1978) or differential scanning dilatometry (D. A. Wilkinson, private communication) in the purple membrane in the range 0–65°C, for general kinetic models (with the notable exception of unidirectional unbranched cycles), the apparent rate constants k_i in Eq. 1 are functions of, not just equal to, the true rate constants in the model. Even if the true rate constants k_i^{true} obey Arrhenius behavior, the apparent rate constants k_i need not, e.g., if $k_i = k_1^{true} + k_2^{true}$. At an early stage in this research a nonlinear least-squares program was developed by R. J. LeVeque that fit many temperatures and wavelengths, and required that the rate constants at different temperatures fall on linear Arrhenius plots. In view of these objections, however, it was felt that this procedure should not be built into such an early stage of the statistical analysis.

Proposition VI: In the temperature range 0–65°C the spectra of the intermediates should not change radically.

A closely related criterion assumes the quantum efficiencies for the bR $\rightleftharpoons$ K light-activated reactions to be independent of temperature. This plus proposition VI leads to proposition VII.

Proposition VII: The fraction cycling *FC* after a fast flash should not depend strongly on temperature.

Proposition VIII: A final assumption that severely restricts possible kinetic models is that the spec-

trum of each intermediate should have a single principal broad maximum (with perhaps some fine structure) in the wavelength range between 380–680 nm.

This assumption is based empirically on the spectra of various retinal compounds (see, e.g., Hara and Hara, 1973, or Sperling, 1973). It has been used previously to propose the N state because the spectrum of M often has a secondary maximum at 520 nm (Lozier et al., 1975).

MATERIALS AND EXPERIMENTAL METHODS

Materials

Purple membrane was prepared from *Halobacterium halobium* cells (strain R_1 or ET1-001) as described by Oesterhelt and Stoeckenius (1974) and stored in a refrigerator (0°C) in 0.01% sodium azide at 1.2–2.9 mg/ml for < 2 mo. Before use, the purple membrane suspensions were diluted with distilled water and the purple membrane reisolated by centrifugation at 39,100 *g* for 20 min. After most of the colorless supernant was decanted, the pellet was resuspended in distilled water to give a stock suspension of purple membrane. This suspension was stored in the refrigerator at 0°C for < 3 wk before use. Before each experiment, 1 ml of the stock suspension was diluted with 1 ml of distilled water and 2 ml of 0.015 M KH_2PO_4/K_2HPO buffer to give a suspension having an optical density of 0.5–0.67 at 570 nm in the light-adapted state in a 1 × 1-cm quartz fluorescence cuvette. The pH of the buffer was determined to be 6.96 ± 0.02, and was not measurably changed when diluted as above with purple membrane. Contamination by "red membrane" was determined by the Ammonyx bleaching assay (Lozier, 1981). Details of the different samples used in this study are given in Table I.

Instrumental

A static absorption spectrum of light-adapted bR was measured at 20 ± 0.5°C in a Cary 14 spectrophotometer with a scattered transmission accessory (Cary Instruments, Fairfield, NJ). Laser flash-induced transmission changes were measured with an apparatus of our own construction. The basic configuration of the apparatus used for the experiments in this study is described in the following text and additional details are given elsewhere (Lozier, 1981). Differences in the configuration between experiments are also mentioned and are listed in Table I.

Actinic light was provided by a Molectron UV1000DL200 nitrogen-laser-pumped dye laser (Molectron Corp., Sunnyvale, CA). The laser beam was focused onto the cuvette center with a combination of a circular and a cylindrical lense. The actinic beam intercepted the monitoring beam at an angle of 90°. Although the actinic beam was nearly plane polarized in the direction perpendicular to the plane containing the actinic and measuring beams, in one experiment a polarizing sheet was placed in the actinic beam to ensure more complete polarization.

The monitoring light beam source consists of a tungsten lamp focused onto the entrance slit of a Jarrel Ash 82-410 1/4 meter monochromator, with the image of the exit slit focused onto the cuvette center (Jarrell Ash Div., Fisher Scientific Co., Waltham, MA). After passing the sample compartment, this monitoring beam is refocused onto a 4-mm-Diam aperture and is incident onto the photocathode of an EMI 9659QB photomultiplier (EMI Gencom Inc., Plainview, NY) which is contained in a Pacific Photometric Instruments (Emeryville, CA) model 62 housing fitted with a high current voltage divider. A combination of 2 × 2-inch interference (Baird Atomic 100A series; Baird Corp., Bedford, MA) and colored glass (Corning Glass Works, Science Products Div., Corning, NY) filters, chosen to pass the monitoring beam while blocking stray actinic light, were placed in a holder between the sample compartment and the photomultiplier. In addition, for most of our data a polarizing sheet was placed between the monochromator and the sample. The orientation of this sheet was chosen to polarize the measuring beam at the "magic" angle $\theta_M = 54.7°$ from the polarization of the actinic beam. The purpose of this polarization scheme was to nullify any effects of tumbling or reorientation of the chromophore upon b_i and to avoid observing absorbance changes that are not intrinsic to the chemical photocycle. Such effects can occur as a result of photoselection of the population $g(\theta)$ of the excited molecules. As the molecules reorient, $g(\theta)$ decays from a $\cos^2\theta$ distribution to a more uniform distribution. Depending on whether the measuring beam is polarized parallel or perpendicular to the actinic beam, the early b_i will be either increased or decreased, respectively,

TABLE I
EXPERIMENTAL CONFIGURATIONS

Experiment	Fermentor	Bacterial strain	% red*	A_{568}^{LA}	Temperature	Time range	Polarization	
							Actinic	Measuring
					(°C)			
1	F-1066	ET1-001	1.4	0.538	20	‡	§	‖
2	DO-43	R1	4.5	0.520	5	‡	vertical	55
3	DO-43	R1	4.5	¶	50	‡	§	50**
4	DO-43	R1	4.5	¶	35	‡	§	50‡‡
5	F-111	R1	9.8	§§	5	‖ ‖	§	50‡‡
6	F-111	R1	9.8	§§	20	‖ ‖	§	50‡‡
7	F-111	R1	9.8	§§	35	‖ ‖	§	50‡‡
8	F-111	R1	9.8	§§	50	‖ ‖	§	50‡‡

*% red is defined as (A_{500} bleached/A_{568} unbleached) × 100%, where A_{500} bleached represents the absorbance of Ammonyx-bleached sample at 500 nm and A_{568} unbleached represents the absorbance of the same amount of light-adapted purple membrane.
‡50 ns → 0.5 s.
§No deliberate polarization; measured polarization (4.63).
‖ No deliberate polarization; polarization varies with wavelength.
¶Not measured, but sample prepared as for experiment 2.
**Polarizer between sample and photomultiplier.
‡‡Polarizer between monochromator and sample.
§§A = 0.670 from spectrum of sample prepared in the same way as sample used in the flash experiment.
‖ ‖ 5°C, 100 μs → 0.4 s; 20°C, 20 μs → 80 ms; 35°C, 20 μs → 40 ms; 50°C, 20 μs → 20 ms.

compared to the later b_i. Only at θ_M are the enhancement factors unity for all times and all intermediates in the cycle. All optical elements from the monochromator exit slit to the photomultiplier were enclosed in a light-tight aluminum box fitted with septa containing apertures for holding the optical components.

The cuvette (a stopperable 1 × 1-cm fluorescence cell) was held by a machined copper block channeled for the circulation of thermostating fluid. The sample temperature was controlled with a Bayley Instrument Co. (Kenwood, CA) model 121 Precision Temperature Controller and was monitored by a steel-sheathed platinum resistance thermometer placed in the sample a few millimeters above the intersection of the monitoring and actinic beams. No effect of the monitoring or actinic beams on the temperature of the sample could be demonstrated. The light energy incident on the sample contributed by the laser was determined by placing a Molectron J3-05 laser monitor near the intersection of the monitoring and actinic beams. The average power in the actinic beam pulses was 0.23 mW. The monitoring beam power, measured with a Kettering Radiant Power Meter (Scientific Instruments, Inc., Lake North, FL), was ~0.01 mW.

Photomultiplier anode current was measured DC coupled on the ±100 mV full-scale range of a Nicolet Explorer IIIA digital oscilloscope or with a Nicolet SD-71B 12 bit 50 kHz ± 250 mV analog-to-digital converter (Nicolet Instrument Corp., Madison, WI). The digital data were averaged over 64 or 256 sweeps and stored on magnetic tape. The beginning of the data acquisition and the triggering of the laser were controlled by a California Avionics Digital Delay Generator, which in turn was externally driven at a frequency of 1.8 Hz. The highest nominal time resolution of our machine was 7 MHz but it was slightly degraded by the photomultiplier rise time, laser triggering jitter, and possibly by drifts in the frequencies of the internal clocks of the instrument. The amplitude resolution of the system was limited by the noise and linearity of the analog-to-digital converters and the shot noise of the photomultiplier signal.

Protocol

With the sample placed in the sample compartment the dark current level was set near the positive end of the voltage scale and for every wavelength the transmitted light level was set near 0 mV by adjusting the lamp wattage and photomultiplier gain. In our experimental protocol the laser is triggered after a constant delay from the beginning of the acquisition period. Thus, our traces have a leading base line representing the light transmittance level before the laser flash. Since the laser flash produces scattered light in the sample compartment which reaches the photomultiplier, it is necesary to determine this laser flash artifact by taking an additional measurement with the measuring beam blocked. This procedure was repeated for every wavelength and temperature. The leading base line with the measuring beam blocked represents the dark-current level, and when it is unblocked represents the 100% transmittance level. To make our measuring scales equivalent at all measuring wavelengths, the digital data were normalized to the transmittance scale using the leading base lines described above. Only the first 20 points of the flash artifact (where all the artifact was confined) were subtracted from its corresponding experimental trace, thus avoiding the addition of unnecessary noise to the data points far removed from the artifact.

From the several hundred data points of each linear flash-artifact-free trace a smaller data set was generated by taking points spaced evenly on a logarithmic time base of 1.3. The first point was taken at t_1 = 350 ns, since this was the earliest time at which the noise due to the flash artifact was not too severe at 480 nm. The second data point was selected from the original linear sweep to be the one for which the time t_2 was closest to 1.3 t_1. In general, the nth data point was selected to be the time t_n closest to $(1.3)^{n-1}\,t_1$. Therefore, this data set consisted of transmittances taken at times which are fairly uniformly spaced on a logarithmic time scale, with the same average number of points in each decade of time. Of course, this is the obvious time base to use for data with several exponential time decays widely separated in time, because each decay is given the same coverage of data points (Austin et al., 1976). It seemed wasteful, however, to throw away completely good data at the 95% of the initially measured times which were not selected for the log time base data. Therefore, the original data points were used to smooth the points used in the log time base according to graduation formulae given by Whittaker and Robinson (1937), which formulae are superior to simple averaging of all data points in an interval. If there were > 20 original data points between a log time base point and either of its neighbors (in log time) then 10 original data points on either side of the log time base point were used to smooth it. However, as there were not as many data points at the beginning of the linear sweeps, fewer original points were used in the graduation formulae in such a way that no original data point was used to smooth more than one log time base point; this ensured against excessive presmoothing of the data which could conceivably obscure small terms in Eq. 1. The transmittance changes were finally converted to absorbance changes for further analysis.

To span > 3.5 orders of magnitude in time, it was necesary with our instrumentation to collect data in three traces, each having a different time resolution. In these cases, consecutive traces were taken to overlap over a time region large enough to provide ~10 pairs of overlapping data points on the slower trace. From these overlapping points an overlap factor was calculated and used to bring the traces to optimal overlap.

ANALYTICAL METHODS

Nonlinear Least-Squares Fitting

With the use of simple graphical techniques, rough estimates of rate constants and even the b_i in Eq. 1 can often be obtained, but for extensive data of the kind required by this paper more sophisticated procedures are in order. The one we have used is due to Golub and Pereyra (1973) and Kaufman et al. (1975) and will be referred to as VARP for variable projection algorithm. Using some sophisticated mathematics, Golub has shown that the fitting problem is separable into a nonlinear part involving only the k_i and not involving the b_i. From the solution of this arduous nonlinear part the b_i are then found by rapid, standard linear least-squares procedures. This is much more efficient computationally than treating all the parameters as nonlinear parameters. This feature is crucial for our problem because we have many b_i and only a few nonlinear parameters, k_i. For example, for S=15 wavelengths and NL=4 components, there are $(S+1) \times NL$=64 total parameters, of which only NL=4 are nonlinear.

We have used the FORTRAN code for VARP supplied by G. H. Golub and R. J. LeVeque with some minor modifications and with an added error analysis of our own design, to be described later. The primary output of VARP is the b_i and the k_i and the norm of the residuals, $RN(\lambda)$, for each wavelength,

$$[RN(\lambda)]^2 = \sum_{i=1}^{N}[A_{bf}(t_i,\lambda) - A_m(t_i,\lambda)]^2, \qquad (2)$$

and the grand norm of the residuals RN

$$RN^2 = \sum_{j=1}^{S}[RN(\lambda_j)]^2, \qquad (3)$$

where N is the number of times and the subscripts bf and m refer respectively, to the best fit and the measured absorbances. Secondary output includes records of the individual residuals at each time and wavelength and a summary of the iteration process. VARP is not especially robust and easily overflows in the early iterations if the supplied initial estimates of k_i are not good enough. Sometimes VARP does not converge, and this is often a sign of an incorrect NL choice. Twice in our experience VARP has converged to a false solution which had an RN larger than given by a different solution found from a different set of starting values; however, we believe that we know how to choose the initial values so as to minimize this erroneous behavior.

Although it is clear that VARP is a sophisticated and powerful tool, we

felt that we needed testing procedures to verify and to understand its capabilities. Accordingly, we wrote a simple program, MOCKDATA, to generate data (also called MOCKDATA) with known characteristics. In one case the MOCKDATA simulates a photocycle with known k_i and extinction coefficients. An even simpler case consists of just a sum of exponentials as in Eq. 1. In both cases a pseudorandom number generator supplies noise at a level chosen by the user to simulate different real data sets. This MOCKDATA was also useful in testing and verifying our spectral calculations described later.

One difficulty with analyzing data one wavelength at a time is that the $b_i(\lambda)$ may be small for some values of i and j, although not for others. When $b_i(\lambda)$ is small, then, as we verified using MOCKDATA, VARP may not find the ith component, but the values of the other k_i and b_i may be affected. Thus a table of k_i vs. λ can be somewhat bewildering (Lozier and Niederberger, 1977). This problem is easily circumvented using VARP on many wavelengths simultaneously. Furthermore, the estimated errors in the k_i decrease since there are more data being analyzed. Since the restriction that the k_i do not depend upon λ is a fundamental constraint, doing the analysis with many λ at a time has only strongly favorable features.

It may be noted in passing that VARP could be advantageously extended to other types of measurements. For example, one could analyze the time development of many resonance Raman lines simultaneously. Furthermore, VARP can simultaneously handle kinetic traces from different kinds of experiments. For example, Keszthelyi and Ormos (1980) have found that the kinetics of the electrical signal appear to be identical to that of the photocycle. However, small but significant differences, which could relate to the rates of proton conduction far removed from the chromophore, might be found using VARP simultaneously on the electrical signals and several wavelengths of the photocycle.

One concern we had with VARP is that it is not programmed, at present, to consider degenerate rate constants in kinetic models. If $k_i = k_j$, then Eq. 1 is no longer the solution of first-order kinetic models, but a new term proportional to $te^{-k_i t}$ is required. Although the chances of pairwise degeneracy is a set of measure zero, it is still of concern what happens near a degeneracy. Mathematically, the solution in Eq. 1 converges to the degenerate solution via the following limit:

$$\lim_{a \to 0} \frac{1}{a}[e^{-k_i t} - e^{-(k_i + a)t}] = te^{-k_i t}. \tag{4}$$

The problem for VARP is that the b_i become large, proportional to $1/a$. Given MOCKDATA with k_1 = constant and $k_2 = k_1 + a$, VARP produced two nearly smooth curves for its estimates of k_1 and k_2, as a function of a, but instead of being straight lines that crossed at $a=0$, the curves repelled each other without crossing. Each curve for k_i joined one of the true lines asymptotically at large positive a and the other true line at large negative a. However, the absolute error at $a=0$ was only 2% in the k. With noisy data the curves were more erratic and show the difficulty in estimating k_i near a degeneracy.

The first decision that must be made in a VARP analysis is the proper number NL of intermediates. An easy and illuminating way to address this question is to look at the graphs of the residuals $R(t,\lambda)$, both as a function of time and as a function of wavelength. For example, for that particular data set at 35°C which does not include the K⟶L decay, the $NL=2$ solution has residual graphs that show a pronounced smooth bump with an amplitude that varies slowly with λ and that appears at the same time for different λ. These nonrandom residuals clearly indicate that another intermediate is required. For $NL=3$ the same test is less conclusive. One can see much smaller bumps, but it is very subjective to say what is random and what is not. A more quantitative test is to examine the estimate for the standard deviation per independent observation

$$\sigma = RN/[N \times S - NL(S+1)]^{1/2}, \tag{5}$$

where $N \times S - NL(S+1)$ is the number of data points at all wavelengths (S in number) and all times (N in number) minus the number of fitted parameters, NL nonlinear and $S \times NL$ linear ones. Testing this on MOCKDATA generated with an actual $NL=3$ gave values of $\sigma = 0.9797$ when VARP was allowed only $NL=2$ exponentials. This improved dramatically to $\sigma = 0.2014$ for $NL=3$ exponentials and barely improved to $\sigma = 0.2011$ for $NL=4$; which is just as would be expected. Similar behavior occurred when the MOCKDATA was generated from $NL=4$ exponentials, even when the amplitudes of the fourth exponential were only ~20% as large as the others. A dramatic decrease from $NL=2$ ($\sigma=0.921$) to $NL=3$ ($\sigma=0.171$) was followed by a smaller improvement for $NL=4$ ($\sigma=0.100$) and by no further improvement for $NL=5$, as expected. Although the σ test would therefore appear to be decisive for finding NL, apparently our real data are subject to systematic error or they disobey Eq. 1, because σ does not reach a constant plateau for finite NL. Thus, other less decisive criteria are used to obtain NL. One criterion is the physical one that b_i should be smoothly varying over the 20-nm-λ grid. Related is the model-dependent criterion that the spectrum should be well behaved. Finally, a more statistical criterion is that k_i should be well determined, as will be discussed next.

Given a trial value of NL it is desirable to estimate the probable errors in k_i. Our procedure is to change k_i by a factor f_i and to recompute the optimal set of b_i. From this we find a new norm of the residuals $RN(f_i)$ and the difference $\Delta_a^2 = RN^2(f_i) - RN^2(1)$, where $RN^2(1)$ is the best-fit value. If one has Gaussian statistics and ignores for the moment the correlations between the different k_i, one expects the relative probability of k_i being replaced by $k_i f_i$ to be $\exp(-\Delta_a^2/2\sigma^2)$. Concerning the statistics, it is interesting to note that Δ_a^2 increases roughly as $(f_i - 1)^2$, but that a much better linear relation holds with $x^2 = (\ln f_i)^2$, as noted by Clore and Chance (1978). Thus one expects the 95% confidence level to be given by that value of f_i for which $\Delta_a = 1.65\sigma$. Incidentally, one might prefer a different approach by computing residuals by comparing the new solution f_i to the best one bf:

$$\Delta_b^2 = \sum_{k,j} [A_{bf}(t_k,\lambda_j) - A_{f_i}(t_k,\lambda_j)]^2, \tag{6}$$

and using Δ_b^2 instead of Δ_a^2. Although the two are not identical, numerically they are not significantly different. To test this error analysis procedure, we applied it to MOCKDATA with known k_i and noise levels. The actual errors, which are the differences between the k_i found by VARP and the k_i from which the noisy data were generated, were comparable to the estimated errors, which are the 95% confidence levels found by the above procedure, provided that the k_i were not close to being degenerate and when the proper value of NL was used. When a smaller value of NL was used, the estimated errors were smaller than the actual errors. When a larger value of NL was used, the estimated errors became much larger and the k_i became poorly determined with probable f_i factors large enough that some pairs of k_i could not be separated.

The above procedure essentially obtains the variances in the k_i. However, the errors in the different k_i are correlated. We have considered such correlations between two k_i taken at a time by varying k_i to $k_i f_i$ and k_j to $k_j f_j$. The appropiate Gaussian variable is $x^2 = (\ln f_i)^2 + (\ln f_j)^2$. The principal axes may consist of linear combinations, such as $\ln f_i - \ln f_j$. The strongest correlations occur when the k_i are nearly degenerate. Indeed, the dependence of Δ_a^2 upon x^2 is no longer linear along the easy principal axis, defined as the one along which Δ_a^2 changes least. This is obvious because as k_i and k_j approach each other on their way to reversing their values to k_j and k_i, respectively, Δ_a^2 must pass through a maximum. Such correlations are accounted for in our error analysis.

Finally, it will be of interest to examine solutions with smaller NL values than indicated by the σ_{NL} test, that is for which $\sigma_{NL+1} < \sigma_{NL}$. The use of smaller NL solutions can be rationalized if it is assumed that there are systematic errors in the data. To accommodate this in the error analysis we suppose that the effective number of observations is less than $N \times S$ by a factor h which is found by requiring that $\sigma'_{NL+1} = \sigma'_{NL}$, where

$$\sigma'_{NL} = RN/[h \times N \times S - NL(S+1)]^{1/2}. \quad (7)$$

The use of σ'_{NL} in obtaining the errors from $\Delta'_a = 1.65\ \sigma'_{NL}$ increases the size of the estimated errors. This new procedure was tested on MOCKDATA. It provides reasonable agreement between the estimated errors and the actual errors for MOCKDATA when a suboptimal choice for NL is made, in which a smaller number of intermediates was used to analyze the data than the number used to create it.

Kinetic Model Analysis

Given any kinetic model of the sort shown in Fig. 1, it is a straightfoward, though sometimes tedious, matter, using Laplace transform techniques, to find the probability, $p_j(t)$, of having state j at time t, given initial conditions. The easiest kinetic model to analyze is an unbranched, unidirectional cycle:

$$1 \xrightarrow{k_1} 2 \xrightarrow{k_2} 3 \xrightarrow{k_3} \ldots\ n \xrightarrow{k_n} \text{bR}. \quad (8)$$

In this model, back-reactions are ignored on the assumption that the energy losses are large enough that the reverse reaction rates are negligible. Usually, one assumes initial conditions, $p_1(0) = FC$, the fraction cycling, and $p_j(0)=0$, $j > 1$, following a fast flash. Owing to instrumental time resolution limitations, one may have $p_1(0) < FC$ and $p_2(0) = FC - p_1(0)$, and, of course, the first state seen with a particular instrument may not be the first state in the photocycle. Fortunately, such nonideal initial conditions make very little difference to spectra calculated for later intermediates, for which $p_j(0)=0$. Of much more concern now is the possibility that, owing to the actinic effect of the measuring beam, there is a substantial fraction cycling in the steady-state even before the fast flash. This would require the kinetic model to be modified to

$$1 \xrightarrow{k_1} 2 \xrightarrow{k_2} 3 \xrightarrow{k_3} \ldots\ \text{bR} \xrightarrow{k_{n+1}} 1. \quad (9)$$

In this case the n apparent rate constants (as would be extracted by VARP) are the roots of $(k_1-z)(k_2-z)\ldots(k_{n+1}-z) - k_1k_2\ldots k_{n+1}$. These rate constants depend upon k_{n+1}, which in turn depends upon the intensity of the measuring beam, so that these are not the same as the rate constants of the model given by Eq. 8, which are just $k_1,k_2\ldots k_n$. Furthermore, the model in Eq. 9 is much more difficult to work with than the one in Eq. 8. Therefore, we avoided such complications by using a measuring beam of low intensity without sacrificing too much signal, which is one reason to use a monochromator in the measuring beam. Our measurements of intensities indicate that the total number of measuring beam photons incident on the sample between flashes is at most 6% the number of actinic beam photons. Knowing that the fraction cycling after the flash is ~6%, the flash rate is 1.8 Hz, the duration of the cycle is ~50 ms at 5°C, and max $\epsilon_{bR}(\lambda)/\epsilon_{bR}(500) = 2.5$, one estimates the fraction cycling due to the measuring beam in the worst case (560 nm) to be only 0.1% and the rate constant k_{NL+1} due to actinic effects of the measuring beam to be only ~0.1% of the slowest intrinsic rate constant at 5°C. This alters the apparent rate constants found by VARP by only ~0.1% from the true rate constants. Nevertheless, this rate constant k_{NL+1} is of the order of 1.2/min, which assures light adaptation during the course of the experiment, even ignoring the actinic flash.

The unidirectional unbranched model in Eq. 8 is solved easily to give

$$p_j(t) = FC \sum_{i=1}^{j} C_{ij}\, e^{-k_i t}, \quad (10)$$

where, $C_{11} = 1$ and for $i<j$

$$C_{ij} = \prod_{m=1}^{j-1} k_m \Big/ \prod_{\substack{n=1 \\ n\neq i}}^{j} (k_n - k_i). \quad (11)$$

From Eq. 10 and 11 the relative absorbances are given by

$$A(t,\lambda) = \sum_{j=1}^{NL} \epsilon'_j(\lambda) p_j(t), \quad (12)$$

where $\epsilon'_j(\lambda)$ is the relative extinction coefficient of the jth state, related by $\epsilon'_j(\lambda) = \epsilon_j(\lambda) - \epsilon_{bR}(\lambda)$ to the absolute extinction coefficient $\epsilon_j(\lambda)$ and the extinction coefficient $\epsilon_{bR}(\lambda)$ of ground state bR. These extinction coefficients are related to the amplitudes $b_j(\lambda)$ found by VARP upon equating Eqs. 12 and 1. The relations are most succinctly stated in matrix form

$$\vec{\mathbf{b}}(\lambda) = FC\,\vec{\vec{C}}\,\vec{\epsilon}'(\lambda), \quad (13)$$

where the vectors are $\vec{\mathbf{b}}(\lambda) = b_1(\lambda),\ldots b_{NL}(\lambda)$ and $\vec{\epsilon}'(\lambda) = \epsilon'_1(\lambda),\ldots\epsilon'_{NL}(\lambda)$ and the matrix elements C_{ij} are given by Eq. 11. If the fraction cycling FC is determined from saturation measurements, then all the $\epsilon'_j(\lambda)$ are determined from the $b_j(\lambda)$. Alternatively, if FC is not known, one may supply a value of $\epsilon'_j(\lambda)$ for one intermediate only at one wavelength only to determine FC. Such values may be obtained from low temperature spectra or from knowledge of an isosbestic or by requiring the smallest absolute $\epsilon_j(\lambda)$ (all j, all λ) to be zero. Our operating procedure was to take $\epsilon_M(420)$ to be 45,000. This choice is not crucial for the conclusions to be drawn in this paper and the reader may easily deduce the effects of other choices from our results by scaling all $\epsilon_j(\lambda)$ according to the ratio

$$[\epsilon_M(420) - \epsilon_{bR}(420)]/[45{,}000 - \epsilon_{bR}(420)]. \quad (14)$$

A computer program called EXTINC was written to compute the extinction coefficients $\epsilon'_j(\lambda)$ and $\epsilon_j(\lambda)$ from Eqs. 11–13, using the output from VARP for the $b_j(\lambda)$ and the C-matrix. EXTINC has no significant numerical error, but it does require that the rate constants k_j be ordered as in Eq. 8. VARP is blind to such ordering in the k_j and may produce them in a permutation different from the actual one. Thus, from the output of VARP there are $NL!$ possible submodels just in the unidirectional, unbranched class of models. Fortunately, when analyzed by EXTINC most of these submodels violate one or more of our propositions and can easily be excluded. In practice, for the bR cycle, when one rate constant is an order of magnitude faster than the others, EXTINC shows that it is the first decay in the cycle; and when a rate constant is much slower than the others it becomes the last decay, although there is no a priori reason why this must be the case and one should not assume it automatically. However, permutation of two nearly equal rate constants sometimes leads to a submodel that has different spectra but that is statistically just as good. With fewer wavelengths and with no estimate of the fraction cycling FC, elimination of many of these possible submodels would be much more difficult. Finally, it is worth noting that permutation of two rate constants, k_{j-1} and k_j, affects only the spectrum of the jth state, as can be verified from the algebraic structure of Eqs. 11–13.

In this paper we shall only consider one additional class of kinetic model, namely unidirectional models with branches directly back to bR.

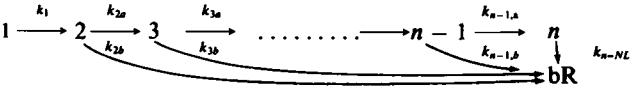

where we define $k_m = k_{ma} + k_{mb}$. For simplicity we shall give the result for only a single branch, so that only one $k_{mb} \neq 0$, but the general result for many branches is easily obtained from generalization of this special case. For a single branch the k_m (not k_{ma} or k_{mb}) are the apparent k found by VARP. Furthermore, the state probabilities of all intermediates before and at the branch are identical to those of the unidirectional, unbranched model with rate constants, $k_1,\ldots k_{NL}$, while those for states beyond the branch are multiplied by k_{ma}/k_m. From this result the relative extinction coefficients are the same before the branch and multiplied by

k_m/k_{ma} after the branch, when compared with the unbranched cycle. Thus the spectra of the intermediates of this additional class of models are easily obtained from the spectra of the unidirectional, unbranched models. It is worth emphasizing here, however, because we use it later, that it is the relative extinctions $\epsilon_j'(\lambda)$, not the absolute extinctions $\epsilon_j(\lambda)$, that are scaled by factors k_m/k_{ma}.

Although we shall not explicitly consider any additional kinetic models in this paper, a brief discussion of the general case is in order. As is well known, most kinetic models have more actual rate constants than apparent rate constants, as is illustrated in the last paragraph where k_m/k_{ma} is a free parameter not determined by analysis of the kinetic data. Although one might then despair that such models can ever be analyzed, in the case of the unidirectional, simple branched cycle discussed above, it turns out to be easy to show that the model is unsatisfactory for every value of k_m/k_{ma}. Although other cases may be equally felicitous, in the general case one must be prepared to try a variety of specific values of the free parameters, some values of which may yield more satisfactory spectra than others. Indeed, concerning this question of free parameters, it might be more desirable to define the term "kinetic model" to mean that enough information is given for the model to be determined from the kinetic data; that is, that values of the free parameters and also permutations of the rate constants be required before a model be considered complete. No matter what the terminology, the computational procedure is clear, although admittedly more tedious for more complex models. With increasing complexity and more free parameters, however, it becomes increasingly likely that kinetic models can be found for which the spectra become well behaved.

RESULTS

This section is divided into three subsections. In the first, results are presented for the data taken with a wide time window, which begins at 350 ns and which includes the K→L decay for $T \leqslant 35$°C. In the remaining two subsections, results are presented for the less noisy narrow window data, which start at times later than the K→L decay. The second subsection is concerned with an analysis based upon $NL=3$ intermediates (L, M, and O) and the final subsection considers $NL>3$ intermediates.

Results for Wide Window Data

Fig. 2 is a plot of relative absorbances vs. log time for λ = 580 nm at 20°C for two different polarization conditions, namely, the measuring beam polarizer vertical and horizontal. The horizontal data have been multiplied by 2.75, which is the theoretical dichroic ratio D for 10% cycling (Nagle et al., 1981). With this factor, the two sets of data agree very well at early times. At later times, the dichroic ratio approaches 1 monotonically. This is most easily interpreted as a spatial disordering, possibly owing to tumbling of the membranes, although this question has not been fully resolved. What can be stated with confidence is that polarization conditions do make a difference and that the use of the magic angle polarizer before the sample is the condition of choice. Fig. 2 also illustrates the general utility of absorbance vs. log t plots. The log t base is clearly preferred to give uniform emphasis to all decays. The use of a linear absorbance scale results, to our initial surprise, in nearly straight lines at times corresponding to k_i^{-1} when the k_i are well separated and the slopes of the lines are proportional to the amplitudes of the decays. These desirable features have been demonstrated analytically (Nagle, 1981).

Fig. 3 shows the Arrhenius plot for K→L decay for various NL. Although this plot is curved, the reason may be due to instrumental truncation of the decay at early times at high temperatures. This truncation is represented in Fig. 3 by the line labeled LID. Because of these errors introduced by the LID the extinction coefficients of the computed spectra also become temperature sensitive as shown in Fig. 4. This temperature effect should not detract from the conclusion that the photocycling, room temperature spectrum of K is given by the 20° spectrum in Fig. 2, which agrees very well with the 5° spectrum, neither of which should be affected by the LID effect. Fortunately, the spectra of other, much slower, intermediates are highly insensitive to errors in k_1 and $\epsilon_k(\lambda)$. The spectrum of K has a maximum near 590 nm, in excellent agreement with published spectra for K near room temperature (Lozier et al., 1975; Goldschmidt et al. 1976), but this spectrum is

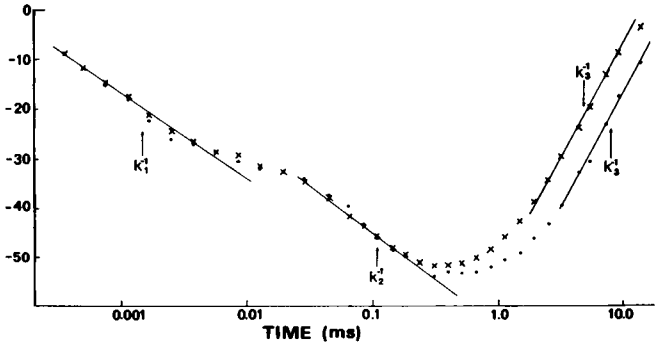

FIGURE 2 Optical absorbance changes at 580 nm and T = 20°C induced by vertically polarized laser flash at 500 nm. The monitoring beam was polarized vertically (×) or horizontally (dots). The absorbance values for the horizontal trace have been multiplied by 2.75. The absorbance of the sample at 580 nm was 0.52. The arrows pointing to the linear portions of the graph are the values of $1/k_j$ found by VARP for NL = 3.

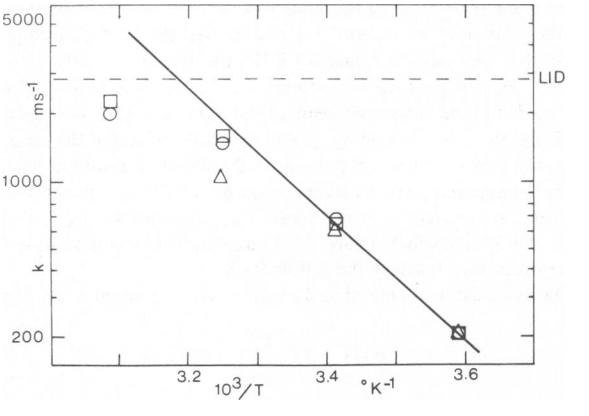

FIGURE 3 Arrhenius plot of fastest component k_1 from wide time window data (experiments 1–4 of Table I) analyzed with NL=3 (△), NL=4 (□), and NL=5 (○) exponential terms. The dashed line indicates the LID which appears to suppress k_1 at 50 and 35°C from a linear relation.

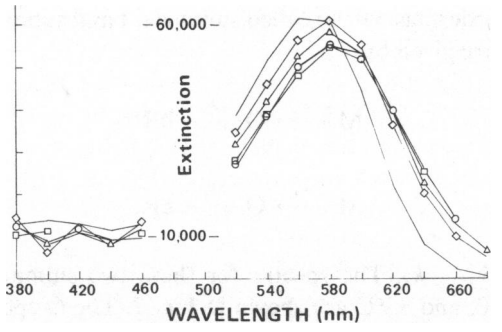

FIGURE 4 Spectrum of the K intermediate (in extinction units) at 5°C (O), 20°C (□), 35°C (△) and 50°C (◇), calculated from wide time window data. The solid line without symbols is the spectrum of bR.

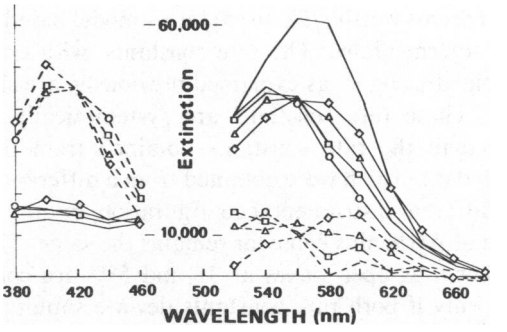

FIGURE 6 Spectra of intermediates L (—) and M (---) calculated from wide window data at 5°C (O), 20°C (□), 35°C (△) and 50°C (◇) on the assumption of an unbranched unidirectional cycle. The solid line without symbols is the spectrum of bR.

considerably blue-shifted from the published spectra for K at 77 K (Lozier and Niederberger, 1977; Becher et al., 1978; Iwasa et al., 1981).

The other, slower, rate constants $k_2, k_3, \ldots k_{NL}$ for these data are shown in Fig. 5. The EXTINC analysis requires the second fastest rate constant k_2 to be the second decay (L→M) in a unidirectional unbranched cycle. Otherwise, Propositions III and IV are violated. Either the $NL=3$ or 4 VARP solutions give excellent linear plots for k_2 in Fig. 5. The L spectra, shown in Fig. 6, do exhibit systematic temperature dependence. However, the percentage temperature dependence of the L spectrum relative to bR, (i.e., $\Delta\epsilon'_L/\epsilon'_L$) is considerably smaller than the temperature

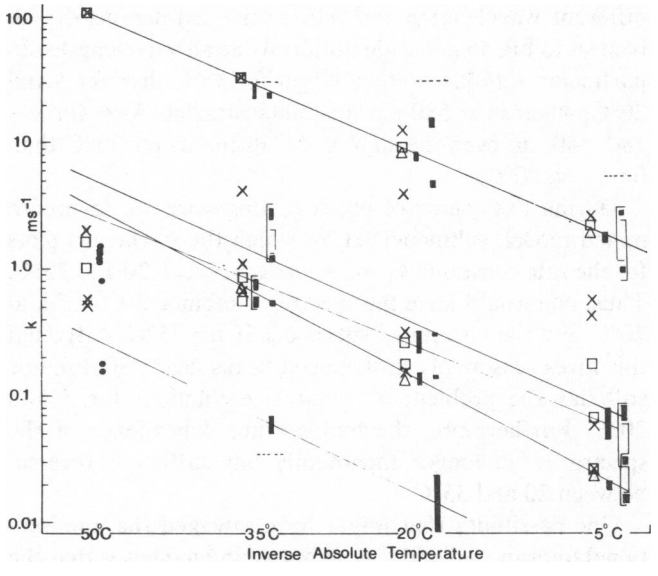

FIGURE 5 Arrhenius plot of slower components from all experiments. The wide time window k_i are shown for $NL=3$ (△), $NL=4$ (□), and $NL=5$ (×), at T = 5, 20, 35, and 50°C. The narrow window k_i were obtained at the same temperatures, but for easier comparison the $NL=3$ results are offset to the right of the wide window k_i and the $NL=5$ results are offset even further to the right at 5, 20, and 35°C. The horizontal dashed lines show the time window for the narrow time window data. Uncorrelated errors are shown by solid bars and correlated errors are shown by brackets. At 50°C nonconvergent VARP results are shown by dots.

dependence of the relative K spectra shown in Fig. 4. The M spectra as a function of temperature, also shown in Fig. 6, also exhibit some variations, $\Delta\epsilon'_M$, but again they are small when compared with the relative extinction coefficients, ϵ'_M.

At this point a decision must be made concerning the naming of the rate constants. Since we do not know which rate constant k_j found by VARP corresponds to which rate constant in Eq. 8 we abandon the naming convention in Eq. 8 in favor of one in which the larger j indicates that k_j was found for the first time in the $NL=j$ solution. The slowest rate constant in this wide window data is k_3. It is always found by VARP before k_4, which is slightly faster at 5 and 20°C. The two rate constants k_3 and k_4 become nearly degenerate at 35°C. In Fig. 5, k_3 and k_4 nearly fall on two straight lines for $T=5$, 20, and 35°C. Unfortunately, there is no way to accommodate the $T=50$°C rate constants to these lines. Moreover, the errors (not shown in Fig. 5) for these fairly noisy data are sufficiently large that firm conclusions are difficult to draw, especially as regards the O spectrum. Nevertheless, the rate constants and the pattern of the O spectrum obtained from this data set are remarkably consistent with those obtained from the less noisy narrow window data to which we turn next.

Narrow Window Data Set

NL=3 Analysis. To clarify the later part of the cycle from M on and to disentangle the rate constants k_3 and k_4, it was felt that less noisy data were needed. With our experimental setup, one easy way to achieve better signal to noise was to avoid the early decay (K→L) with rate constant k_1 and begin the data acquisition at times between L and M. This resulted in σ about four times smaller and signals two-thirds as large, for a net improvement in signal to noise of ~3. We were surprised to find, using the σ test discussed in Methods, that the number of statistically significant rate constants was > $NL=3$; i.e., corresponding to states L, M, and O which in the fast data set corresponds to $NL=4$ and states K, L, M, and O. However, since the additional terms have small amplitudes

$b_j(\lambda)$, it seems worthwhile to explore a model based on only $NL=3$ intermediates. The rate constants, with error bars determined using σ', as explained previously, are shown in Fig. 5. These rate constants are systematically slightly slower than the rate constants obtained from the wide window data, which were obtained from a different sample and a different instrumental configuration, but the general pattern of Arrhenius behavior remains the same. The error bars shown as open boxes at 35 and 5°C are correlated errors; only if both rate constants deviate simultaneously to those ends shown by the connecting lines of the boxes or to the other pair of opposites, are such deviations within the 95% confidence level. Thus, the Arrhenius lines for k_3 and k_4 at 35°C are outside the 95% probable range, even though both pass through the open box. The data at 50°C did not include the L→M (k_2) decay and VARP got into a degenerate solution and did not converge. However, the scattered nonconvergent results shown are consistent with the wide window results except for the new very slow rate constant which will be discussed below in the next subsection. Unfortunately, the 50°C data for this narrow window data set could not be analyzed in any way to make it fit a pattern including the other data, perhaps owing to the loss of the L→M decay; we shall therefore ignore them.

The L spectra for this data set are very similar to those shown in Fig. 6 for the wide window data set and will not be shown again. The M spectra, shown in Fig. 7, appear to be less noisy than the M spectra of the wide window data set shown in Fig. 6, but are otherwise compatible, although $\epsilon_M(\lambda)$ may be somewhat smaller in the 520–580 nm region for this data. It may be noted in passing that the effect of using an $\epsilon_M(420)$ smaller than 45,000 is to increase $\epsilon_M(\lambda)$ in the 520–580 nm region.

Given the unidirectional unbranched model, there are two orderings of the final rate constants, k_3 and k_4, which fit the data equally well, and which must be considered.

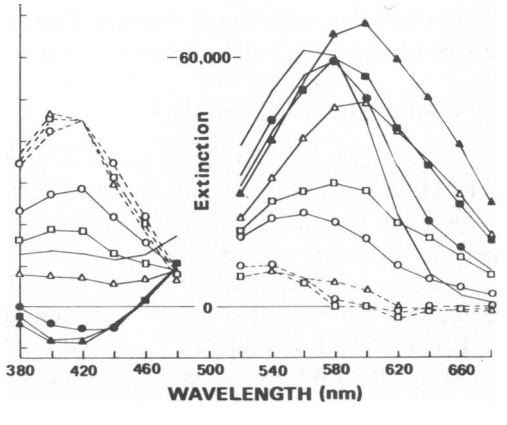

FIGURE 7 Spectra of intermediates M (---) and O (—) calculated from narrow time window data at 5°C (○,●), 20°C (□,■), and 35°C (△,▲). For reference, the solid line without symbols is the spectrum of bR. The O spectra are shown with solid lines for submodel I (filled symbols) and submodel II (open symbols). The M spectra are the same for both submodels.

These orderings will be called submodel I and submodel II, which are given by

$$M \xrightarrow{k_3} O \xrightarrow{k_4} bR, \qquad (I)$$

$$M \xrightarrow{k_4} O \xrightarrow{k_3} bR, \qquad (II)$$

where $k_3 < k_4$. The spectra for these two submodels at $T=5$, 20, and 35°C are shown in Fig. 7. The O spectra of submodel I (closed symbols) exhibit strong peaks near 580 nm. However, the peaks increase dramatically in size as temperature increases in violation of Proposition VI. The most serious difficulty with submodel I is that $\epsilon_O(\lambda)$ is strongly negative for λ=400–440 nm in violation of Proposition III. A temperature-dependent branch from M back to bR only leads to larger negative extinctions. Furthermore, it cannot eliminate the temperature dependence of the peaks above 500 nm because the relative extinctions $\epsilon'_O(\lambda)$ do not scale uniformly for all wavelengths.

The spectra of submodel II are also shown in Fig. 7. These spectra are strongly temperature dependent, in violation of Proposition VI, and they exhibit bimodality with one minor peak below 500 nm and another minor peak above 500 nm, in violation of Proposition VIII. Unlike submodel I, however, the O spectra for submodel II are always positive. A temperature-dependent branch from M back to bR does not improve the spectra, as is easily seen because the isosbestics with bR occur at different wavelengths and the relative extinctions ϵ'_O with respect to bR do not scale uniformly at all wavelengths. In particular, $\epsilon'_O(660)$ is much larger for 35°C than for 5 and 20°C, whereas at 580 nm it is much smaller. Also, for λ = 380–440 nm even the sign of ϵ'_O is different for 35°C than for 5 and 20°C.

During the course of much of this work we favored a mixed model, submodel III, in which the Arrhenius plots for the rate constants k_3 and k_4 cross between 20 and 35°C. Thus, one would have the spectra of submodel I for 5 and 20°C and the spectra of submodel II for 35°C. Although this gives reasonably pronounced peaks near 580 nm, one still has the problem of negative extinctions for 5 and 20°C. Furthermore, the temperature dependence of the spectra is no longer monotonic, but suffers a reversal between 20 and 35°C.

One possibility that might have salvaged the unidirectional unbranched and simple branching models is that the true solution need not be the best solution found by VARP but only needs to have the k_i within the error bars shown in Fig. 5. Therefore, we explored likely variations of the k_i within these limits. The best possibility was to choose k_3 and k_4 more nearly degenerate at 35°C. This produces an O spectrum intermediate between the two 35°C spectra shown in Fig. 7, with a maximum more nearly equal in size to those of the 5 and 20°C spectra of submodel I. The spectrum is red-shifted for λ>500 nm, however, and it

becomes nearly zero at 420 nm. The probable variations in the 5 and the 20°C spectra are smaller and do not appreciably alleviate the mismatches. In particular, the spectra for $\lambda<500$ nm remain strongly negative for 5 and 20°C.

While none of the unidirectional unbranched submodels meets all our criteria, it is still of interest to know the fraction of intermediates present as a function of time for submodels I and II. This information is given in Fig. 8 for the L, M, and O states at 20°C. The maximum fraction in M is never as large as 1. As expected, the maximum fraction in M is larger for submodel I than for submodel II, whereas the maximum fraction in O is larger for submodel II. It is important to emphasize that both submodel I and submodel II represent the data equally well, but the spectra of the intermediates are different for the two models. Also, notice that in submodel I it is the decay of O, not the rise of O, which has the same apparent rate as the decay of M, even though this submodel is unbranched and unidirectional.

The fraction cycling, *FC*, predicted by EXTINC for the unidirectional, unbranched model is 0.061, 0.056, and 0.052 at 5, 20, and 35°C, respectively. These values of *FC* would be increased by ~19% if we had used $\epsilon_M(420) = 40{,}000$ instead of 45,000. It is encouraging that the temperature variation in *FC* is not large, in agreement with Proposition VII. In addition, these values of *FC* obey Proposition IV, where a rough independent estimate of *FC* is obtained as follows. The maximum fraction cycling, *MFC*, for a short, intense flash which saturates the sample and establishes photoequilibrium between bR and K is given by

$$MFC = \left(1 + \frac{\phi_k \epsilon_k(500)}{\phi_{bR} \epsilon_{bR}(500)}\right)^{-1}, \qquad (17)$$

where the ϕ are the quantum efficiencies. From published ϕ (Becher and Ebrey, 1977) and $\epsilon_k(500)$ (Iwasa et al., 1981) or our $\epsilon_k(500)$, this gives $0.43 < MFC < 0.53$ for a 500-nm actinic flash. The difficulty in using this result is that our laser does not have enough intensity to achieve saturation. Indeed, from the theory of photoselection we

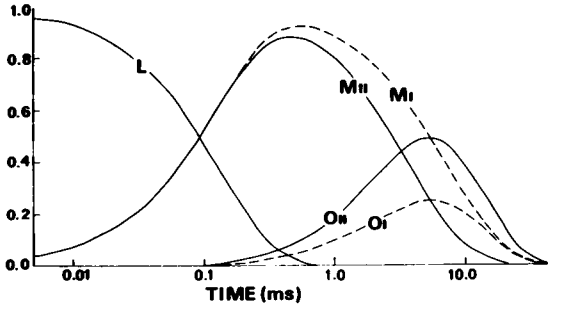

FIGURE 8 The relative concentrations at 20°C of various intermediates L, M, and O as a function of time for the two submodels I (---) and II (—). The L concentration is the same in both submodels.

believe that saturation will be achieved only very slowly with increasing intensity I.[1] In particular, even with an unpolarized actinic beam, those molecules with transition moments nearly parallel to the beam will require much higher light intensities to saturate than those with moments perpendicular. For a polarized actinic beam and the measuring beam polarized at the magic angle we have derived the formula

$$A = A_{max}\,[1 - (\pi/4c_1I)^{1/2}\, erf(\sqrt{c_1 I})], \qquad (18)$$

where $c_1 I$ is the relative actinic intensity, so that c_1 is a fitting parameter, and *erf* is the error function. This formula indicates that the saturation is achieved slowly as $I^{-1/2}$. (The derivation also allows us to plot the dichroic ratio D as a function of light intensity. D falls rapidly as I is increased from 0. For intensities which yield only 10% of saturation or ~5% cycling, typical of our later experiments, D has already fallen from 3 to ~2.8.)

Although we have not made full use of this approach to obtain a precise independent estimate of *FC*, we can conclude that *FC* was certainly < 10% for the narrow time window measurements, and this suffices to exclude various submodels, especially when $NL=5$ is considered in the next subsection.

NL>3 Analysis. VARP produces fits to the data, when given $NL=4$ or 5 intermediates (after K), which are statistically better than the $NL=3$ fit as judged by the σ test. While the fourth and fifth exponentials have considerably smaller amplitudes, b_j, than the first three, nevertheless, the b_j are fairly smoothly varying on the 20-nm wavelength grid. In contrast, the amplitudes of the sixth exponential found when $NL=6$ are much more random as a function of λ. The Arrhenius plot does not look regular for the fourth exponential in Fig. 5, in violation of Proposition V. However, it is noteworthy that the same pattern as a function of temperature for the fourth rate constant emerges from the wide window data set (see above, first subsection) and from earlier data sets produced by Richard H. Lozier alone. In contrast the fifth rate constant has not been seen previously in this lab. At first it was thought to be a problem with the base line, but manual plotting of the data also shows this very slow, weak decay, which is more evident at higher temperatures. In fact VARP did not find it at 5°C, and from the error bars in Fig. 5 it is evident that it is only marginally present at 20°C. However, the fact that simple manual data plotting reveals its existence at 35°C indicates that it should be considered at 35 and 20°C. Since this fifth exponential is much weaker than the fourth, clearly that one must be considered too, even though Proposition V would exclude

[1] J. F. Nagle, S. M. Bhattacharjee, L. A. Parodi, and R. H. Lozier. Effect of photoselection upon saturation and the dichroic ratio in flash experiments upon effectively immobilized systems. Paper in preparation.

it. The runs-of-signs test (Swed and Eisenhart, 1943) also supports this conclusion that $NL=5$ intermediates are required to fit the data.

Let the rate constants be numbered according to $k_2>k_5>k_4>k_3>k_6$ (k_1 is not seen in this data set). With $NL=5$ there are $5!=120$ submodels to be considered. At all temperatures, k_6 must come last in an unidirectional cycle in order that the spectra do not violate the negativity criterion, Proposition III. This results in a state, called P by Gillbro (1978), which has almost the same spectrum as bR, differing by at most $\epsilon'_P(600) = 2{,}000$ at 35°C. At both 20 and 35°C $\epsilon_P(\lambda) < \epsilon_{bR}(\lambda)$ for $\lambda>540$ nm, and the relative spectrum reverses sign only for 35°C. Since the sign of such small differences is hard to resolve, one can only conclude that the differences are small.

Let the submodels, corresponding to different orderings of the rate constants, be identified as a sequence of five numbers, where the locations of the numbers in the sequence identify their locations in the unidirectional unbranched cycle submodel. For example, [25436] corresponds to the submodel where each successive rate is slower than the last. Submodel [25436] is distinguished by having a second M-like state, in addition to the P state already described. The two M states will be called M_1 and M_2 in order of their appearance in the cycle. That M_i which has smaller $\epsilon(420)$ has larger $\epsilon(540)$. This is M_1 at 35°C and M_2 at 5 and 20°C. The two $\epsilon_M(\lambda)$ are very similar in magnitude at 5°C but differ significantly at 20 and 35°C. The L and O spectra of submodel [25436] are very similar, including their temperature dependence, to the L and O spectra of the $NL=3$ submodel II, which in the present notation, could be called submodel [243].

Submodel [25346] is similar to submodel I or to [234] for $NL=3$ in that the k_3 and k_4 rates are reversed. Furthermore, the O spectra for [25346] have the same problems of large negative spectra for $\lambda = 400$–440 nm and strong temperature dependence of the peaks, the location of whose maxima range from 570 nm at 5°C to 620 nm at 35°C. Another submodel we tried is [52436]. For 5 and 20°C this model has the M state, which appears immediately after L as usual. Following M, it has a bimodal state, which we may call N with a spectrum intermediate between M and L both for high and low wavelengths. The main problem with this submodel is that the fraction cycling FC is too high and variable, in violation of Propositons IV and VII, with $FC=0.20$ for 20°C and 0.13 for 5°C. This submodel also works very badly at 35°C with the totally unrealistic value of $FC=0.45$. This is because the rate constants k_2 and k_5, which are swapped in this model, differ much more at 35°C than at the lower temperatures. Similarly, submodel [24536], which swaps rate constants k_4 and k_5, is much better behaved for 35°C than at 5 and 20°C. For 35°C another N state with a peak at 570 nm is produced between M and O. The spectra for [52436] at 5 and 20°C are somewhat similar to the spectrum of [24536] at 35°C. However, the fraction cycling varies dramatically from 0.20 to 0.13 to 0.053 upon increasing temperature, in violation of Proposition VII. Additional submodels we explored violate our criteria even more and hence they will not be considered here.

DISCUSSION

The primary goal of this paper is to elucidate a procedure for testing kinetic models of the photocycle of bR from flash photolysis data. The technical breakthrough that allows us to develop a more extensive and refined procedure than those used by previous researchers is a nonlinear least-squares fitting routine (VARP), developed by Golub and co-workers (1973) and adapted by R. J. LeVeque to handle data taken at many wavelengths. From the output of VARP (rate constants and amplitudes) the procedure calculates the model-dependent spectra of the intermediates and the fraction cycling using a particular kinetic model. It is important to emphasize that the amplitudes alone are not amenable to analysis because they involve a complicated mixture of the intermediates. The spectra are amenable to analysis, however, and in our procedure they are subjected to a number of tests, which we have called propositions. Some of our propositions, such as Proposition III (spectra must be positive) and IV (fraction cycling must be less than unity) are very strong statements, which must be satisfied. Even though these are so obvious, nevertheless, they are effective in reducing the number of models to be considered. Other propositions, such as Proposition I (first-order kinetics), II (smooth spectra), VI (temperature-independent spectra), and VII (temperature-independent fraction cycling), could conceivably be violated, but they seem to us to be fairly strong criteria for a good kinetic model to satisfy. We consider Proposition VIII (one principal peak) to be somewhat weaker but still likely to be valid. We regard Proposition V (linear Arrhenius plots) to be the weakest and indeed we do not use this proposition in this paper.

As an illustration of our procedure we have applied it, using new data obtained with careful consideration of the possible complications of photoselection, to the unidirectional unbranched kinetic model and also to the unidirectional kinetic model with simple branching straight back to bR. It was our hope that the unidirectional unbranched model with $NL=4$ intermediates (K,L,M, and O) would prove to be a satisfactory representation of the photocycle of bR. In particular, we had not been convinced by previous arguments that required simple branching because full consideration of rate reversal (i.e., $k_{M\to O} < k_{O\to bR'}$, [submodel I], or a mixed submodel, in which $k_3 - k_4$ reverses sign near 35°C [submodel III]) had not been given. In this paper, in addition to considering these possibilities, considerable effort was expended to estimate errors; even if the most probable spectra are ill behaved, statistically possible spectra might have satisfied all our criteria. Furthermore, use of the larger σ' errors for the

narrow window data seems to us to give the unidirectional unbranched cycle every benefit of the doubt. Nevertheless, the spectra of this model fail to meet our criteria. Even the L and M states, for two different data sets, are somewhat temperature dependent in a fairly systematic way, in violation of Proposition VI. As previously noted, however, the most dramatic failure is the O spectra. With any ordering of the slower rates, to give submodels I, II, or III, the spectra violate Proposition VI and either Propositions III (submodels I and III) or Proposition VIII (submodel II).

One possible salvation of the unidirectional unbranched model was that more intermediates might be required, and this is supported by our statistical analysis of the narrow window data, which calls for two additional intermediates. The hardest intermediate to distinguish, called P by Gillbro (1978), because its spectrum is close to bR, appears very late in the cycle and does not alleviate the problem of O. The other intermediate usually appears as a second M-like state, but the Arrhenius behavior of the rate constant is strongly nonlinear, in violation of Proposition V. This new intermediate also does not alleviate the problem of O and its spectrum is even more strongly bimodal than the first M, in violation of Proposition VIII. Other permutations of the rates produce additional submodels, but these are even worse candidates, usually violating Proposition VII or even the stronger Propositions II or IV.

We also considered the class of unidirectional kinetic models with simple branching straight back to bR. Despite the extra free parameter in such models, all the difficulties mentioned in the last paragraph for the unidirectional unbranched model also are present in the simple branching models.

It is possible, as suggested by W. Stoeckenius (private communication), that perhaps the cycle is more complicated only when the sample is under nonphysiological conditions and/or that the small amounts of 13-*cis* retinal-containing bR recently found in fully light-adapted samples complicate the data (Mowery et al., 1979). Accordingly, experiments in high salt are planned and the 13-*cis* bR contribution will either be minimized or taken into account in the analysis by considering models with independent cycles. Even if these experiments indicate a simpler cycle, it is important to report the kinetics under the distilled water conditions , because most workers have so far employed similar conditions and the effects of low ionic strength must be explained and may contribute substantially to our understanding of the reaction mechanism. Unfortunately, it seems likely that the kinetic model under any conditions is more complex than had been hoped. The worst possibility would be that the kinetics are not first-order, so that even Proposition I does not hold. A less dramatic departure from expectations is that the true model may involve back-reactions, dead-end side paths, and/or nonsimple branching. Of course, there are a large number of such models, even before considering the many more submodels due to permutations of the rates. It is quite likely that the problem will not be solved quickly, but systematic exploration of the various kinetic models will undoubtedly lead to improved agreement with experiment. The positive result of this paper is development of a procedure or methodology that makes such explorations systematic. We feel strongly that such methodology is crucial in unraveling such complex and important questions as the photocycle of bacteriorhodopsin.

We wish to thank R. J. LeVeque and G. H. Golub for providing the VARP program, W. Stoeckenius for his steadfast encouragement of this project and for helpful comments on the manuscript, and W. Niederberger and L. Eisenstein for helpful discussions at the beginning of this research.

Financial support was provided to Dr. Lozier and Dr. Parodi by National Institutes of Health grant GM-27057 and National Aeronautics and Space Administration grant NSG-7151, and to Dr. Nagle by National Science Foundation grant DMR 78-10226 and the Guggenheim Foundation.

Received for publication 29 January 1981 and in revised form 31 July 1981.

REFERENCES

Applebury, M. L., K. S. Peters, and P. M. Rentzepis. 1978. Primary intermediates in the photochemical cycle of bacteriorhodopsin. *Biophys. J.* 23:375–382.

Austin, R. H., K. W. Beeson, S. S. Chan, P. G. Debrunner, R. Downing, L. Eisenstein, H. Frauenfelder, and T. M. Nordlund. 1976. Transient analyzer with logarithmic time base. *Rev. Sci. Instrum.* 47:445–447.

Becher, B., and T. G. Ebrey. 1977. The quantum efficiency for the photochemical conversion of the purple membrane protein. *Biophys. J.* 17:185–191.

Becher, B., F. Tokunaga, and T. G. Ebrey. 1978. Ultraviolet and visible absorption spectra of the purple membrane protein and the photocycle intermediates. *Biochemistry.* 17:2293–2300.

Blatz, P., and J. Mohler. 1975. Effect of selected anions and solvents on the electronic absorption, nuclear magnetic resonance, and infrared spectra of the *N*-retinylidene-*n*-butylammonium cation. *Biochemistry.* 11:2304–2309.

Clore, G. M., and E. M. Chance. 1978. The kinetics and thermodynamics of the reaction of solid-state fully reduced membrane-bound cytochrome oxidase with carbon monoxide as studied by dual-wavelength multichannel spectroscopy and flash photolysis. *Biochem. J.* 175:709–725.

Dencher, N., and M. Wilms. 1975. Flash photometric experiments on the photochemical cycle of bacteriorhodopsin. *Biophys. Struct. Mech.* 1:259–271.

Edgerton, M. E., and C. Greenwood. 1979. Evidence for a model of regeneration of a protonated species, bR, from a phototransient, M, in the photochemical cycle of bacteriorhodopsin from *Halobacterium halobium. Biochem. Soc. Trans.* 7:1075–1077.

Gillbro, T. 1978. Flash kinetic study of the last steps in the photo-induced reaction cycle of bacteriorhodopsin. *Biochim. Biophys. Acta.* 504:175–186.

Gillbro, T., A. N. Kriebel, and U. P. Wild. 1977. On the origin of the red emission of light adapted purple membrane of *Halobacterium halobium. FEBS (Fed. Eur. Biochem. Soc.) Lett.* 78:57–60.

Goldschmidt, C. R., M. Ottolenghi, and R. Korenstein. 1976. On the primary quantum yields in the bacteriorhodopsin photocycle. *Biophys. J.* 16:839–843.

Golub, G. H., and V. Pereyra. 1973. The differentiation of pseudoin-

verses and nonlinear least-squares problems whose variables separate. *SIAM (Soc. Ind. Appl. Math.) J. Numerical Analysis.* 10:413–432.

Hara, T., and R. Hara. 1973. Biochemical properties of retinochrome. *In* Biochemistry and Physiology of Visual Pigments. H. Langer, editor. Springer-Verlag, New York. 181–191.

Honig, B., A. D. Greenberg, U. Dinur, and T. G. Ebrey. 1976. Visual-pigment spectra: implications of the protonation of the retinal Schiff base. *Biochemistry.* 15:4593–4599.

Iwasa, T., F. Tokunaga, and T. Yoshizawa. 1980. A new pathway in the photoreaction cycle of trans-bacteriorhodopsin and the absorption spectra of its intermediates. *Biophys. Struct. Mech.* 6:253–270.

Jackson, M. B., and J. M. Sturtevant. 1978. The phase transitions of the purple membranes of *Halobacterium halobium. Biochemistry.* 17:911–915.

Kaufmann, K. J., P. M. Rentzepis, W. Stoeckenius, and A. Lewis. 1976. Primary photochemical processes in bacteriorhodopsin. *Biochem. Biophys. Res. Comm.* 68:1109–1115.

Kaufman, L. 1975. A variable projection method for solving separable nonlinear least squares problems. *Bit.* 15:49–57.

Keszthelyi, L., and P. Ormos. 1980. Electrical signals associated with the photocycle of bacteriorhodopsin. *FEBS (Fed. Eur. Biochem. Soc.) Lett.* 109:189–193.

Korenstein, R., B. Hess, and D. Kuschmitz. 1978. Branching reactions in the photocycle of bacteriorhodopsin. *FEBS (Fed. Eur. Biochem. Soc.) Lett.* 93:266–270.

Kung, M. C., D. Devault, B. Hess, and D. Oesterhelt. 1975. Photolysis of bacterial rhodopsin. *Biophys. J.* 15:907–911.

Lozier, R. H. 1981. Rapid kinetic optical absorption spectroscopy of bacteriorhodopsin photocycles. *Methods Enzymol.* In press.

Lozier, R. H., R. A. Bogomolni, and W. Stoeckenius. 1975. Bacteriorhodopsin: a light-driven proton pump in *Halobacterium halobium. Biophys. J.* 15:955–962.

Lozier, R. H., and W. Niederberger. 1977. The photochemical cycle of bacteriorhodopsin. *Fed. Proc.* 36:1805–1809.

Marcus, M., and A. Lewis. 1978. Resonance Raman spectroscopy of the retinylidene chromophore in bacteriorhodopsin (bR570), bR560, M412 , and other intermediates: structural conclusions based on kinetics, analogues, models, and isotopically labled membranes. *Biochemistry.* 17:4722–4735.

Mowery, P. C., R. H. Lozier, Y.-T. Tseng, Quae Chae, M. Taylor, and W. Stoeckenius. 1979. Effect of acid pH on the absorption spectra and photoreactions of bacteriorhodopsin. *Biochemistry.* 18:4100–4107.

Nagle, J. F. 1981. Upon the optimal graphical representation of flash data from photochemical systems obeying first order kinetics. *Photochem. Photobiol.* 33:937–939.

Oesterhelt, D., and W. Stoeckenius. 1974. Isolation of the cell membrane of *Halobacterium halobium* and its fractionation into red and purple membrane. *Methods Enzymol.* 31:667–678.

Sherman, W. V., R. Korenstein, and S. R. Caplan. 1976. Energetics and chronology of phototransients in the light response of the purple membrane of *Halobactrium halobium. Biochim. Biophys. Acta.* 430:454–458.

Sherman, W. V., R. R. Eicke, S. R. Stafford, and F. M. Wasacz. 1979. Branching in the bacteriorhodopsin photochemical cycle. *Photochem. Photobiol.* 30:727–729.

Sperling, W. 1973. Conformations of 11-*cis* retinal. *In* Biochemistry and Physiology of Visual Pigments. H. Langer, editor. Springer-Verlag, New York. 19–28.

Stoeckenius, W., R. H. Lozier, and R. A. Bogomolni. 1979. Bacteriorhodopsin and the purple membrane of *Halobacteria. Biochim. Biophys. Acta.* 505:215–278.

Swed, F. S., and C. Eisenhart. 1943. Tables for testing randomness of grouping in a sequence of alternatives. *Annals. Math. Stat.* 14:66–87.

Whittaker, E. T., and G. Robinson. 1937. The calculus of observations. Blackie and Son, London. 2nd edition.